Journal of Applied Remote Sensing

RemoteSensing.SPIEDigitalLibrary.org

Vegetation isoline equations with first- and second-order interaction terms for modeling a canopy-soil system of layers in the red and near-infrared reflectance space

Munenori Miura
Kenta Obata
Hiroki Yoshioka

SPIE.

Vegetation isoline equations with first- and second-order interaction terms for modeling a canopy-soil system of layers in the red and near-infrared reflectance space

Munenori Miura,[a] Kenta Obata,[b] and Hiroki Yoshioka[a,*]
[a]Aichi Prefectural University, Department of Information Science and Technology, 1522-3 Ibara, Nagakute, Aichi 480-1198, Japan
[b]National Institute of Advanced Industrial Science and Technology, Institute of Geology and Geoinformation, Central 7, 1-1-1, Higashi, Tsukuba, Ibaraki 305-8567, Japan

Abstract. A previously proposed vegetation isoline equation suffers from errors if the soil background of a canopy layer is bright. These errors arise from the truncation of the second- and higher-order terms that represent photon interactions between the canopy and the soil. An isoline equation that includes a second-order interaction term is introduced. The equation was initially derived by explicitly including a second-order interaction term in both the red and near-infrared (NIR) reflectance spectra (symmetric approximation). We also examined an alternative model in which the interaction term was included only in the NIR band (asymmetric approximation). In this model, the derived isolines tend to shift upward (overcorrection effects). Numerical experiments revealed that the errors in the isoline obtained by the asymmetric approximation were reduced in magnitude to nearly one-fifth of the errors in the previously proposed method. Its accuracy was higher than that of the symmetric approximation, despite the fact that the asymmetric approximation included fewer terms than the symmetric approximation. The improved model accuracy resulted from the overcorrection effects, which compensated for the truncation error. With the simplicity and improved accuracy, the current isoline equations provide a good alternative to the previous approach. [DOI: 10.1117/1.JRS.9.095987]

Keywords: vegetation isoline; leaf area index; fraction of vegetation cover; canopy radiative transfer model; inversion.

Paper 15278P received Apr. 16, 2015; accepted for publication Oct. 14, 2015; published online Nov. 18, 2015.

1 Introduction

Biophysical parameter retrieval from remotely sensed reflectance spectra is a fundamental goal in the field of land remote sensing. Qin et al.[1] categorized the available retrieval algorithms into four groups based on the approaches taken: (1) techniques that relied on a spectral vegetation index (VI) and its correlation with biophysical parameters, such as the leaf area index (LAI);[2–7] (2) algorithms that used lookup tables;[8,9] (3) neural networks;[10–12] and (4) direct inversions of numerical models [e.g., models of radiative transfer (RT)] using optimization methods.[1,9,13–15] These approaches present advantages and disadvantages over other approaches in terms of accuracy, computational costs, complexity, and applicability. The common feature of all categories of approach is that a better model increases the accuracy of the retrieved parameters. For this reason, significant efforts have been applied toward improving the accuracy of physical and numerical models.

The concept of vegetation isolines[2,16–20] forms the basis of the spectral VI,[2,7,18,20] which has been widely used as a proximity measure (model) of surface biophysical parameters.[21] The isoline concept has been used as an analytical tool for investigating the influence of the soil on the retrieved parameters.[22–28] From this standpoint, vegetation isoline equations provide a model for

*Address all correspondence to: Hiroki Yoshioka, E-mail: yoshioka@ist.aichi-pu.ac.jp

the relationship between reflectances at different wavelengths. Several reports have attempted to use isolines in the analysis of the VI [24,28] and in parameter retrieval.[29,30] Recently, these relationships were applied to intercalibration studies of the VI values obtained from different sensors.[31–33] Thus, the accuracy of the vegetation isoline equation must be improved in order to improve parameter retrieval algorithms and better understand the factors that affect intercalibration studies.

Yoshioka et al.[34] found that the derived isoline by the isoline equations loses accuracy in intermediate ranges of the LAI. Loss of accuracy in the isoline equation arises from truncations of the terms that correspond to multiple interactions among the photons reflected from the canopy layer (at the bottom surface) and the soil surface. These terms are referred to as higher-order interaction terms[34] in this study. The isoline equations derived by Yoshioka et al. [24,34,35] retain the interaction terms up to the first-order terms. The truncation, however, simplifies the derivation and yields a final form that is useful as an analytical tool.[24,28,31–33] One drawback of this truncation, however, is the loss of accuracy, which must be improved while simultaneously retaining the simplicity of the model. This study seeks to do just this.

We conducted a series of pilot studies[36–38] to explore possible improvements to the higher-order terms in the isoline equations. Derivations were developed for use in several cases. Three model issues have yet to be clarified. First, the relationship between the previously derived isoline, which includes a first-order interaction term, and the newly derived isoline, which includes higher-order interactions, is not yet understood. Second, the mechanism by which the errors were reduced upon inclusion of the higher-order term has not yet been identified. In some cases, isolines containing fewer interaction terms to describe one of the two bands showed significantly better accuracy. This mechanism must be explored systematically. This study examines these matters from an analytical and numerical perspective. The isoline equation derived here is even simpler than the equation introduced in the pilot studies; thus, this equation may be readily applied to new analyses. Finally, numerical procedures for determining the isoline parameters were not discussed in the pilot studies. These matters require further study for application purposes.

The objective of this study is to improve the first-order isoline equation by including second-order interaction terms while maintaining the model simplicity. This objective was achieved through a novel approach. Instead of retaining the second-order interaction terms of both the red and near-infrared (NIR) bands, we retained the term only for the reflectance of the NIR band. The asymmetric treatment of the second-order interaction significantly improved the model accuracy without sacrificing the simplicity of the derived expression. This study describes the formal steps, which used to derive the improved version of the vegetation isoline equation and validate its accuracy by conducting numerical experiments based on a coupled leaf and canopy RT model, PROSAIL.[39]

The remainder of this discussion presents a review of a previously derived vegetation isoline equation,[24,34] referred to as a first-order isoline equation in this study. Two forms of higher-order approximations are derived. The results of numerical experiments using an RT model are then shown to evaluate the degree to which the accuracy was improved by the introduction of the higher-order approximations. The mechanism by which the accuracy was improved by the approximations is discussed in detail. Finally, the findings of this study are summarized.

2 Analytical Model and First-Order Vegetation Isoline

2.1 *Analytical Canopy Reflectance Model*

This study begins with an analytical form of the top of the canopy (TOC) reflectance model, which has been used extensively in this field of study:[40]

$$\rho_\lambda = \omega\rho_{v\lambda} + \omega\frac{T_\lambda^2 R_{s\lambda}}{1 - R_{s\lambda}R_{v\lambda}} + (1-\omega)R_{s\lambda}, \tag{1}$$

where the variables and notations mainly follow those given in Refs. 24 and 34, except for the fraction of vegetation cover (FVC) represented by ω in this study. The variable ρ_λ represents the

TOC reflectance at the wavelength λ, $\rho_{v\lambda}$ represents the "pure" canopy reflectance, which can only be obtained by assuming perfect absorbance beneath the canopy layer, $R_{s\lambda}$ and R_{v_λ} represent the bihemispherical reflectance of the soil and canopy layers, respectively. The variable $R_{v\lambda}$ is somewhat special among these variables because it represents the albedo of the bottom surface of the canopy layer. The details of the model are illustrated in Fig. 2 of Ref. 34. T_λ^2 represents the two-way transmittance of the canopy layer at the indicated wavelength, λ. We next defined the area-averaged two-way transmittance at a point:

$$\overline{T_\lambda^2} = \omega T_\lambda^2 + 1 - \omega. \tag{2}$$

The word "area-averaged" indicates that the bare soil region, $(1-\omega)$, provides "perfect" two-way transmittance properties, and the averaged transmittance of the partially vegetated area may be modeled using a weighted average of T_v^2 and 1.0, with weighted values of ω and $(1-\omega)$. In the following section, we briefly explain the vegetation isoline equation introduced previously.[24,34]

2.2 *Vegetation Isoline Equation with a First-Order Interaction Term in the Red–Near-Infrared Reflectance Subspace*

The isoline equation introduced in this subsection is referred to as the first-order isoline because only a single interaction term with the soil surface is included.

The model was derived by explicitly including the first-order interaction term as the second term of the right-handside (RHS) of Eq. (3),

$$\rho_\lambda = \omega\rho_{v\lambda} + \omega T_\lambda^2 R_{s\lambda} + \frac{\omega T_\lambda^2 R_{s\lambda}^2 R_{v\lambda}}{1 - R_{s\lambda}R_{v\lambda}} + (1-\omega)R_{s\lambda}, \tag{3}$$

where the second term of the RHS in Eq. (3) indicates the first-order interaction term. The second and higher interaction terms, represented by the third term of the RHS, are further defined as a truncated-order term:

$$O(R_{s\lambda}^2) = \frac{T_\lambda^2 R_{s\lambda}^2 R_{v\lambda}}{1 - R_{s\lambda}R_{v\lambda}}. \tag{4}$$

Equation (3) can be simplified using Eq. (2):

$$\rho_\lambda = \omega\rho_{v\lambda} + \overline{T_\lambda^2} R_{s\lambda} + \omega O(R_{s\lambda}^2). \tag{5}$$

Two equations were used to describe the red (denoted by the subscript R) and NIR wavelengths (N):

$$\rho_R = \omega\rho_{vR} + \overline{T_R^2} R_{sR} + \omega O(R_{sR}^2), \tag{6}$$

$$\rho_N = \omega\rho_{vN} + \overline{T_N^2} R_{sN} + \omega O(R_{sN}^2). \tag{7}$$

The soil line assumption of Ref. 41 was applied:

$$R_{sN} = aR_{sR} + b, \tag{8}$$

where a and b represent the slope and offset of the soil line, respectively. Equations (6)–(8) were used to eliminate the soil reflectances R_{sR} and R_{sN} to obtain the first-order approximated vegetation isoline equation:

$$\rho_N = a\gamma_1\rho_R + D_1 + \epsilon_1, \tag{9}$$

where γ, D, and ϵ_1 are defined by

$$\gamma_1 = \overline{T_N^2}/\overline{T_R^2}, \tag{10}$$

$$D_1 = b\overline{T_N^2} + \omega(\rho_{vN} - a\gamma_1\rho_{vR}), \tag{11}$$

$$\epsilon_1 = \omega[O(R_{sN}^2) - a\gamma_1 O(R_{sR}^2)]. \tag{12}$$

Finally, we obtained an approximated form of the vegetation isoline equation by truncating the higher-order interaction term:

$$\rho_N \approx a\gamma_1\rho_R + D_1. \tag{13}$$

The first-order isoline model suffers from truncation errors. For example, Yoshioka et al.[34] indicated that the truncation error increases at higher soil reflectance values, and the relative error can reach 5%. Their findings suggest that the errors in the retrieved biophysical parameters, calculated based on the isoline formula, can reach the same magnitude. The truncation errors in the isoline formula should, therefore, be minimized to obtain more accurate parameter retrievals using the isolines.

The truncation error pattern obtained from the first-order isoline model was numerically characterized using a RT model PROSAIL.[39] Figure 1 shows the first-order isoline and reflectance spectra simulated using the model in the red and NIR reflectance subspaces. The empty circles denote the simulated reflectance, which was considered to be a "true" spectrum. The solid lines indicate the first-order isoline at various LAI values of the pure canopy component ranging from 0 to 4 at intervals of 0.5. The left and right figures present the results obtained from different FVC (ω) values: full coverage ($\omega = 1$) or half coverage ($\omega = 0.5$), respectively. A detailed description of the simulation conditions is provided in the latter section. These results confirmed that the error (the discrepancy between the empty circles and the solid lines) in the first-order isoline could be reproduced numerically using the model presented in this study.

The error trend was characterized by plotting the distance between the isolines and the true spectra, as shown in Fig. 2, at LAI = 1.0 (solid line) and LAI = 4.0 (dashed line) for both the fully covered and partially covered cases. The error was plotted as a function of the soil reflectance in the red band. The figure clearly reveals two characteristics: first, the error increased as the soil became brighter. Second, the error at LAI = 1.0 always exceeded that obtained for LAI = 4.0. Because these trends have been analyzed previously,[24,34] we summarize the conclusions briefly: (1) the influence of the higher-order interaction terms increased for brighter soils and (2) this influence first increased and then decreased as the canopy thickened.

The error could be reduced to some extent by adjusting the higher-order terms. The next section discusses the derivation steps that are used to obtain the second-order approximated reflectance and a new isoline equation referred to as the "asymmetric order isoline" in this study.

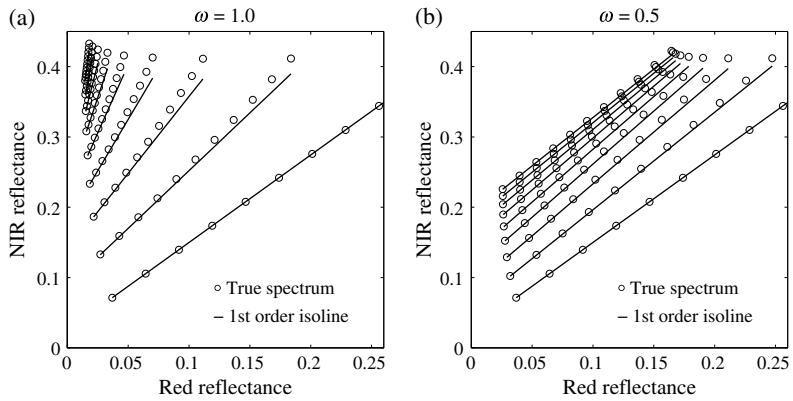

Fig. 1 First-order vegetation isolines and simulated reflectance spectra obtained using PROSAIL. The value of the fraction of vegetation cover (FVC) represented by ω was assumed to be (a) unity, representing a fully covered case and (b) 0.5, representing a partially covered case.

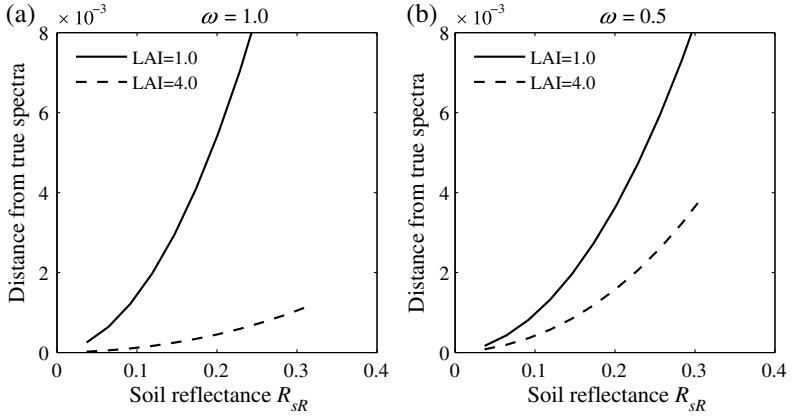

Fig. 2 Distance between the first-order isoline and the true reflectance spectrum shown in Fig. 1 for (a) $\omega = 1.0$ and (b) $\omega = 0.5$.

3 Second-Order Approximation and Asymmetric Order Isoline

3.1 *Parametric Form of the Second-Order Approximated Reflectance Spectra*

The second-order interaction term could be explicitly separated from the higher-order term in Eq. (3) using the approach taken to separate the first-order term. Specifically, the interaction terms were retained up to the second order for both the red and NIR spectra in Eq. (3). The resulting equation then becomes

$$\rho_\lambda = \omega\rho_{v\lambda} + \overline{T_\lambda^2}R_{s\lambda} + \omega T_\lambda^2 R_{v\lambda}R_{s\lambda}^2 + \omega O(R_{s\lambda}^3), \tag{14}$$

where

$$O(R_{s\lambda}^3) = \frac{T_\lambda^2 R_{s\lambda}^3 R_{v\lambda}^2}{1 - R_{s\lambda}R_{v\lambda}}. \tag{15}$$

We next rewrote Eq. (14) to describe the red and NIR bands using the subscripts R and N to obtain

$$\rho_R = \omega\rho_{vR} + \overline{T_R^2}R_{sR} + \omega T_R^2 R_{vR}R_{sR}^2 + \omega O(R_{sR}^3), \tag{16}$$

$$\rho_N = \omega\rho_{vN} + \overline{T_N^2}R_{sN} + \omega T_N^2 R_{vN}R_{sN}^2 + \omega O(R_{sN}^3). \tag{17}$$

The soil line in Eq. (8) was used to obtain the reflectance spectrum to a second-order approximation, as represented by the following form with R_{sR} as a parasite parameter:

$$\begin{bmatrix}\rho_R\\ \rho_N\end{bmatrix} = \begin{bmatrix}\overline{T_R^2} & \omega T_R^2 R_{vR}\\ a\overline{T_N^2} + \omega 2abT_N^2 R_{vN} & \omega a^2 T_N^2 R_{vN}\end{bmatrix}\begin{bmatrix}R_{sR}\\ R_{sR}^2\end{bmatrix} + \omega\begin{bmatrix}\rho_{vR}\\ \rho_{vN} + b\overline{T_N^2}/\omega + b^2 T_N^2 R_{vN}\end{bmatrix} + \omega\begin{bmatrix}O(R_{sR}^3)\\ O(R_{sN}^3)\end{bmatrix}. \tag{18}$$

The last term could be neglected to obtain a parametric representation of the approximated second-order spectrum. This form was used only in the numerical experiments to evaluate the isoline equation, as discussed in Sec. 3.2.

3.2 *Isoline Equation Obtained by Asymmetrically Truncating the Higher-Order Interactions*

The previous subsection discussed the retention of the higher-order interaction terms up to the second-order terms for both the red and NIR bands. In this subsection, we include the second-order interaction term only in the description of the NIR band, and the red band is approximated up to the first-order interaction term.

A system of equations was obtained using Eqs. (6), (8), and (17), in which the soil reflectances were eliminated. Algebraic manipulations yielded the final results:

$$\rho_N = a^2\zeta\rho_R^2 + a(\gamma_1 + \delta_1)\rho_R + D_1 + \delta_0 + \epsilon_2, \tag{19}$$

where

$$\zeta = \omega T_N^2 R_{vN} / (\overline{T_R^2})^2, \tag{20}$$

$$\delta_0 = \zeta(b\overline{T_R^2} - \omega a\rho_{vR})^2, \tag{21}$$

$$\delta_1 = 2\zeta(b\overline{T_R^2} - \omega a\rho_{vR}), \tag{22}$$

$$\epsilon_2 = \omega O(R_{sN}^3) + a^2\omega^2\zeta[O(R_{sR}^2)]^2 - a\omega[2a\zeta\rho_R + \gamma_1 + 2\zeta(b\overline{T_R^2} - a\omega\rho_{vR})]O(R_{sR}^2). \tag{23}$$

Neglecting ϵ_2 from Eq. (19), we have

$$\rho_N \approx a^2\zeta\rho_R^2 + a\gamma_2\rho_R + D_2, \tag{24}$$

where

$$\gamma_2 = \gamma_1 + \delta_1, \tag{25}$$

$$D_2 = D_1 + \delta_0. \tag{26}$$

4 Results of the Numerical Simulations

4.1 *Parameter Settings Used in the Numerical Experiments*

A series of numerical experiments was conducted using the canopy RT model PROSAIL.[39] This model consists of the leaf model PROSPECT[42] and the canopy model SAIL;[43] thus, two types of input parameter were required. Numerical experiments were conducted using the set of input values provided with the code, except that the three input parameters—LAI, leaf angle distribution (LAD), and soil factor—were set as follows. The soil factor was obtained from the mixture ratio of the wet and dry soil spectra provided with the code. The parameter ranges of the three parameters were as follows. LAI was varied from 0.0 to 4.0 at 0.5 intervals (9 levels), and the soil factor was varied from 0.0 to 1.0 at 0.1 intervals (11 levels). During the numerical experiments, six LAD models (planophile, erectophile, plagiophile, extremophile, spherical, and uniform distributions) were assumed. (This section focuses on the case of a spherical LAD, as a representative case, for brevity.) Finally, the obtained reflectance spectra were linearly mixed with the pure soil reflectance spectra using the fraction of green cover (ω) as a weight. The parameter ω was varied from 0.0 to 1.0 in 0.1 intervals (11 levels). The total number of spectra used to model each LAD was 1089. In the analysis, we assumed that the reflectances at 655 and 865 nm provided representative values of the red and NIR bands in this study. This choice of wavelength pair corresponded to the center of the red and NIR bands obtained from the Landsat 8 operational land imager sensor.

The other input parameters provided with the code were fixed as follows. For the SAIL part of the code, the parameter describing the hot spot (hspot) was set to 0.01. The solar zenith, observation zenith, and relative azimuth angle were set to 30, 10, and 0 deg, respectively. For the PROSPECT part of the code, chlorophyll-a and -b, carotenoid, and the leaf mass per area were assumed to be 40, 8, and 0.009 in g/cm^2, respectively. The equivalent water thickness was set to 0.01 cm, and the brown pigment content was assumed to be zero. Finally, the leaf mesophyll structure (N) was assumed to be 1.5 (the equivalent number of layers).

4.2 *Numerical Procedure Used for the Isoline Parameter Retrieval and the Error Estimation*

The isoline parameters used in Eqs. (9) and (19) were computed from $T_{v\lambda}^2$ and $\rho_{v\lambda}$, which were determined using the algorithm described in Ref. 34. This algorithm required two hypothetical simulations in which the soil was assumed to be "spectrally flat," with a zero reflectance value, or the soil was assumed to have a medium reflectance value over the entire wavelength range. In addition to $T_{v\lambda}^2$ and $\rho_{v\lambda}$, the asymmetric order approximated isoline, Eq. (19), required a value of R_{vN} to define ζ. R_{vN} was determined by conducting an additional simulation in which the soil was assumed to be spectrally flat and even brighter than was assumed in the simulation used to determine $T_{v\lambda}^2$. The assumption of brighter soil increased the photon contributions of the higher-order interactions. The parameter R_{vN} was determined by solving Eq. (17) for R_{vN} and using T_{vN}^2 and ρ_{vN}, which were computed prior to R_{vN}. With these variables in hand, the isoline parameters γ_1, D_1, γ_2, D_2, ζ, δ_0, and δ_1 were obtained. In summary, three hypothetical simulations were conducted to determine the isoline parameters that corresponded to spectrally flat soil at three different brightness levels.

The errors in the isolines and the approximated reflectance spectra were estimated by computing the distance from the true spectra. Note that the error in the isolines should be equal to the distance between the true reflectance spectrum (which includes all higher-order interaction terms) and the "isoline" represented by Eqs. (9) and (19), corresponding to the first-order and asymmetric order isolines, respectively. Even if a spectrum approximated using a model based on truncated higher-order terms was far from the true spectrum, the error could be zero provided that the "isoline" passed through the point of the true spectrum in the red–NIR reflectance subspace. This distance was employed as a measure of the error because the error in the biophysical parameter retrieval obtained using the isoline reached zero numerically under conditions in which the true spectrum point coincided with the isoline. The goal of isoline determination is to identify the conditions under which the isoline coincides with the true spectra.

4.3 *Comparison of the Accuracy Across the Three Approximations*

The performances of the two types of isoline, namely, the first-order and second-order isolines, were compared with the true and second-order reflectance spectra obtained in the red–NIR reflectance subspace. Figure 3 represents the isolines as solid lines. The first-order [Eq. (9)] and the asymmetric order [Eq. (19)] isolines are plotted as black and red lines, respectively. The empty circle represents the true spectra obtained directly from PROSAIL and corresponds to the spectra represented by Eq. (1). The crossmark was used to indicate the second-order approximated reflectance spectra [Eq. (18)]. The isolines were compared at two values of the vegetation cover: (a) $\omega = 1.0$ and (b) $\omega = 0.5$.

These figures reveal that the asymmetric isolines (red lines) provided much better approximates for the true spectra (empty circles) than the first-order isolines (black lines) over the entire LAI range. The error in the asymmetric order isoline was smaller than that obtained from the first-order isoline. Further analyses in this subsection (Table 1) and the next subsection (Fig. 6) indicated that the asymmetric isolines were even closer to the true spectra than the second-order approximated reflectance spectra (crossmarks) over the full spectral range. This result is, to some extent, surprising because the error in the second-order approximated spectrum was expected to be smaller than the error obtained from the asymmetric isoline, in which one of the bands (the red

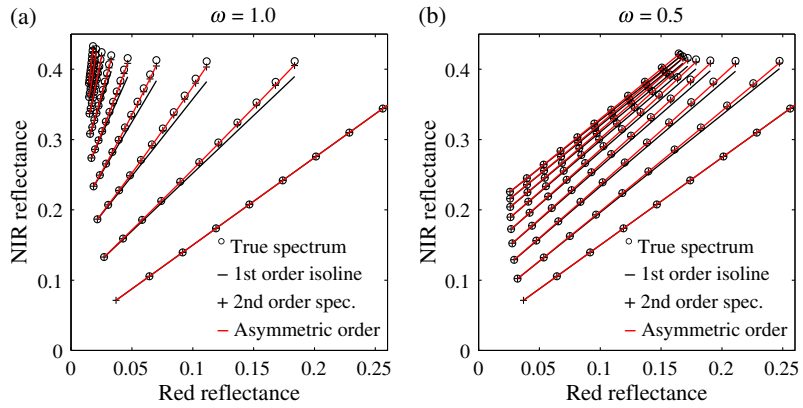

Fig. 3 First-order isoline (black line) defined by Eq. (9), and the asymmetric isoline (red line) defined by Eq. (19), with the second-order reflectance spectra (cross mark) computed using Eq. (18) and the true spectra (empty circle) computed using PROSAIL. The value of the FVC represented by ω was assumed to be (a) unity, representing a fully covered case and (b) 0.5, representing a partially covered case.

band in this study) was approximated to the first order instead of to the second order. This result will be further discussed later in this section.

The errors obtained from the two isolines and the second-order reflectance spectra were directly compared, and the distance between these isolines and the spectra obtained from the true values (including all higher-order terms) are plotted as a function of the soil reflectance R_{sR} for the four combinations of LAI and ω (Fig. 4). The errors obtained from the first-order isoline, second-order reflectance, and asymmetric order isoline are denoted using different colors. Figures 4(a) and 4(b) show the results obtained for the fully covered case, with LAI = 1.0 and 4.0, respectively. Figures 4(c) and 4(d) show the results obtained for the half-covered case. These figures indicated that (1) the error over R_{sR} was high at high values of R_{sR} and (2) in most cases, the errors of the asymmetric isoline were the smallest among the three models over the range of R_{sR}. This result indicates that the accuracy of the asymmetric isoline dramatically improved over the entire range of R_{sR}. Again, recall that the asymmetric isoline used a first-order approximated reflectance to model the red band, whereas a second-order reflectance was used to model the second-order interaction terms in both the red and NIR bands. The error in the second-order reflectance (blue line) was expected to be smaller than the error obtained from the asymmetric isoline (red line). These results could be explained in terms of the relationship between the overcorrection and the truncation error. This mechanism is described in detail below.

Before discussing these surprising results, we will analyze the error trend by investigating the error distributions obtained from the simulations conducted using combinations of the three input parameters (LAI, FVC ω, and soil reflectance R_{sR}) employed in this study. Figure 5 shows a histogram of the errors obtained from the three approximations. The figure reveals that the asymmetric order isoline errors were clustered at lower errors, unlike the errors of the other two approximations, and very few simulations provided errors of 1.0E − 3. On the other hand, the errors of the first- and second-order isoline reflectance simulations were uniformly distributed at distances exceeding 1.0E − 3. These results confirmed that the asymmetric order isoline outperformed the other two approximations.

The model performances were further validated by varying the LAD. The experiments compared the results obtained by assuming six different LAD models: planophile, erectophile, plagiophile, extremophile, spherical, and uniform distributions. The error values were averaged over the entire range of the three parameters (LAI, ω, and R_{sR}). These results are summarized in Table 1, which lists the standard deviation and the maximum values obtained in all cases. The table indicates that the average error of the asymmetric order isoline was much smaller (by nearly one order of magnitude) than the average error of the first-order isoline for all LAD cases. The table also reveals that the performance of the asymmetric order isoline was better than that of the second-order reflectance in terms of the average, standard deviation, and the maximum value.

Table 1 Average, standard deviation, and maximum differences between the true reflectance spectra and the three cases of the isoline/reflectance spectra. The differences were computed by assuming six types of leaf angle distribution (LAD): planophile, erectophile, plagiophile, extremophile, spherical, and uniform distributions.

	First order isoline	Second order spectrum	Asymmetric isoline
		LAD: planophile	
Mean	1.93E – 03	8.53E – 04	3.46E – 04
STD	2.47E – 03	1.33E – 03	5.06E – 04
MAX	1.30E – 02	8.08E – 03	2.56E – 03
		LAD: erectophile	
Mean	2.93E – 03	1.92E – 03	8.44E – 04
STD	3.68E – 03	2.84E – 03	1.16E – 03
MAX	1.85E – 02	1.60E – 02	5.79E – 03
		LAD: plagiophile	
Mean	1.57E – 03	5.53E – 04	2.16E – 04
STD	2.06E – 03	8.89E – 04	3.23E – 04
MAX	1.10E – 02	5.60E – 03	1.62E – 03
		LAD: extremophile	
Mean	1.74E – 03	6.33E – 04	2.47E – 04
STD	2.26E – 03	1.01E – 03	3.68E – 04
MAX	1.18E – 02	6.22E – 03	1.84E – 03
		LAD: spherical	
Mean	1.95E – 03	8.79E – 04	3.57E – 04
STD	2.51E – 03	1.37E – 03	5.21E – 04
MAX	1.32E – 02	8.31E – 03	2.65E – 03
		LAD: Uniform	
Mean	1.65E – 03	5.85E – 04	2.28E – 04
STD	2.15E – 03	9.38E – 04	3.41E – 04
MAX	1.13E – 02	5.86E – 03	1.71E – 03

Table 1 supports the above findings (e.g., that the asymmetric order isoline performed better than the other models), derived in Figs. 4 and 5. Section 4.4 analyzes the detailed mechanisms underlying this trend.

4.4 *Error Reduction Mechanisms Using the Second-Order Isoline*

The numerical results presented above indicate that the asymmetric order isoline model was more accurate than the reflectance approximated up to the second-order interaction terms, despite the fact that the latter included a greater number of terms in the red band than did the asymmetric order isoline. This trend is not easy to understand intuitively, but it appeared to result from the tendency of the model to overcorrect by a degree that was approximately equal to the order of magnitude of the truncation error in the isoline.

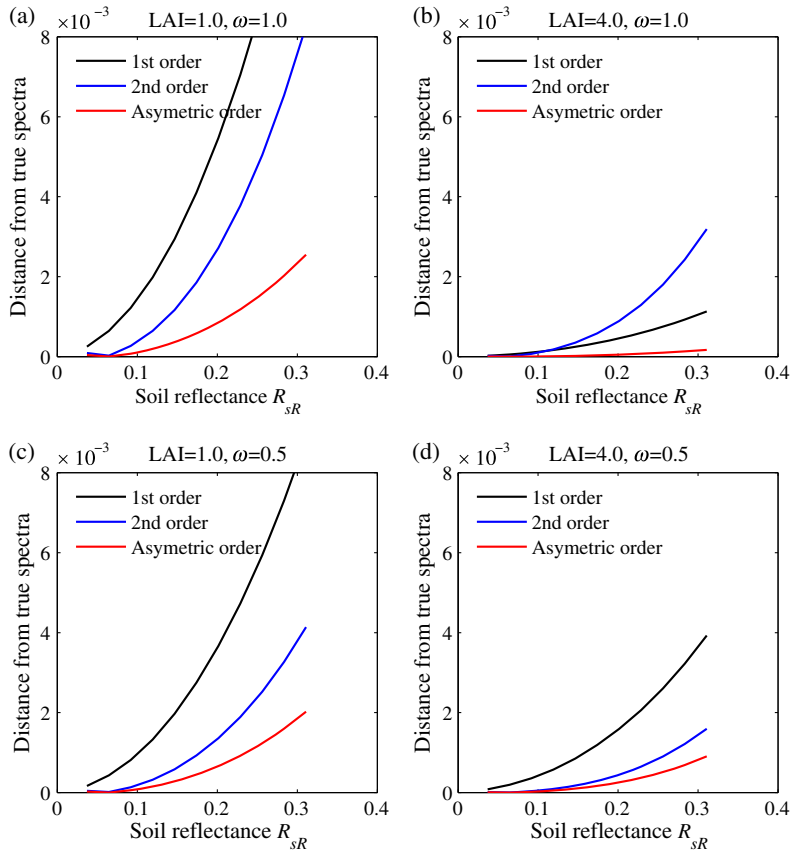

Fig. 4 Distance between the first-order isoline, second-order reflectance spectrum, or the asymmetric isoline and the corresponding true reflectance spectra, as a measure of the error shown in Fig. 3 at four combinations of leaf area index (LAI) and ω: (a) LAI $= 1.0$; $\omega = 1.0$, (b) LAI $= 4.0$; $\omega = 1.0$, (c) LAI $= 1.0$; $\omega = 0.5$, and (d) LAI $= 4.0$; $\omega = 0.5$.

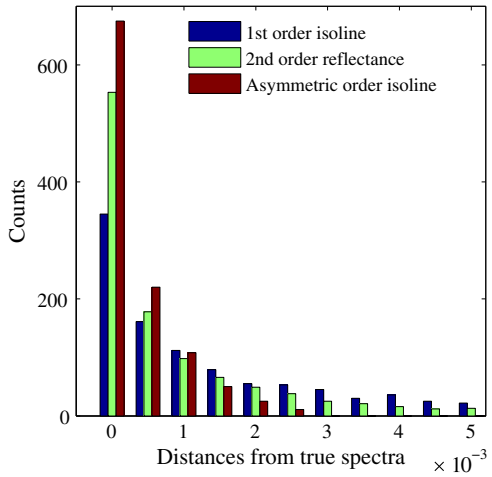

Fig. 5 Histogram of the errors obtained from the first-order isoline, second order reflectance, and asymmetric order isoline. The total number of simulated cases was 1089 = (9 discrete values of LAI) × (11 values of FVC, ω) × (11 values of soil reflectance R_{sR}), assuming a spherical leaf angle distribution.

We further examined the model performances by plotting the four reflectance spectra: (1) the true spectrum computed directly using PROSAIL; (2) the first-order approximated reflectance; (3) the second-order approximated reflectance; and (4) the asymmetric order approximated reflectance using two types of vegetation isoline (first-order isoline and asymmetric order

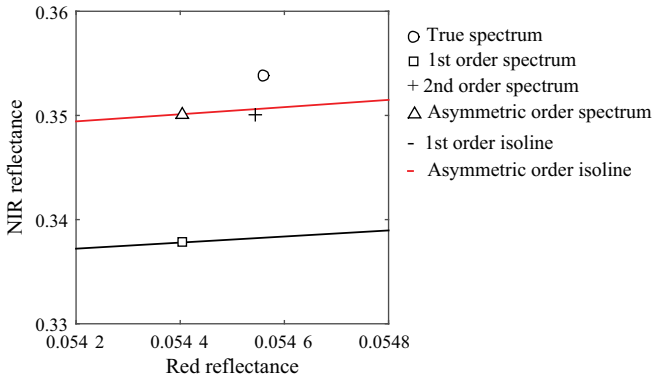

Fig. 6 Comparison of the four approximated reflectance spectra: true spectrum calculated using PROSAIL (circle), first-order approximated spectrum (square), second-order approximated spectrum (cross), and asymmetric order approximated spectrum (triangle), with the two isolines (first-order, black line, and asymmetric order, red line.) The value of LAI $= 2.0$ and full canopy coverage ($\omega = 1.0$) was assumed.

isoline). Figure 6 shows a limited region of the red-NIR reflectance subspace to illustrate the differences between the four predicted spectra. This part of the subspace corresponds to the results obtained at LAI $= 2.0$ for the case of full canopy coverage.

Figure 6 reveals that the closest spectrum to the true spectrum (denoted by the circle) is the second-order approximated reflectance, denoted by the crosses. The asymmetric isoline represented by the red line is even closer to the true spectrum, whereas the asymmetric order approximated reflectance spectrum (triangle) is further from the true spectrum compared to the second-order approximated spectrum. Recall that the errors are measured as the distance between the true spectrum (circle) and the model spectra. Because the distance to the isoline (red line) was smaller than the distance between the true spectrum and the second-order approximated spectrum (cross), the error of the asymmetric isoline was surely smaller. Therefore, these results are consistent with the trend described in the previous subsection.

This trend could be understood as resulting from an overcorrection to the NIR band in the asymmetric approximation and the truncation error in the isoline. In the asymmetric case, the inclusion of a second-order term only in the NIR band overcorrected the spectrum upward in the direction from the first-order spectrum (square), as illustrated in Fig. 7. The overcorrection of the NIR band shifted the asymmetric order approximated spectrum (triangle) from the position of the first-order approximated spectrum (square) parallel to the NIR axis instead of toward the true reflectance spectrum (circle). Fortunately, this shift direction and distance compensated for the truncation error. As a result, the isoline of the asymmetric approximation (red line) ran through the subspace between the true (circle) and second-order approximated spectra (cross). In summary, the overcorrection of the NIR band and the truncation error in the NIR band nicely canceled each other out, thereby shifting the isoline (red) upward into the subspace to decrease the distance between the true spectrum and the isoline.

5 Discussion and Conclusions

The truncation of higher-order interaction terms presents a major limitation to isoline models based on a first-order approximation, although this truncation can simplify the final expression. The simplicity of the analytical form is advantageous for analytical and numerical investigations of parameter retrieval algorithms, such as the LAI, FVC, as well as of proximity measures, such as the spectral VI. The accuracy of the vegetation isoline models may be increased by including the second-order interaction terms in both the red and NIR reflectances; however, the derived expression was rather complex, thereby reducing the utility of the model as a tool for analytical and numerical studies. This study took a unique approach: instead of including the second-order terms in both the red and NIR bands, this study included the term only in the NIR reflectance.

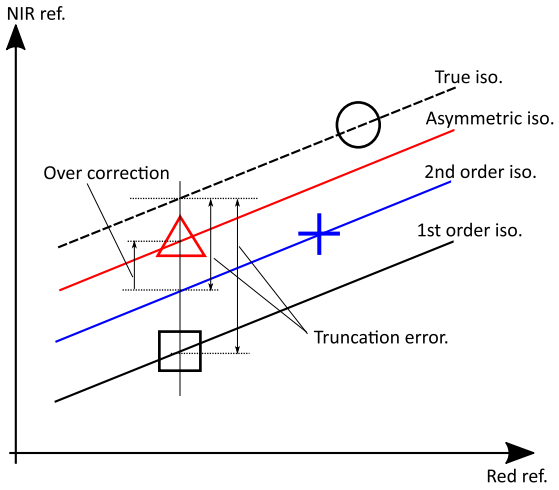

Fig. 7 Illustration of the error reduction mechanism in the asymmetric order approximated isoline.

The final form of the derived asymmetric isoline is rather simple; thus, it can be easily altered, similar to the previously derived first-order isoline. This model, however, dramatically reduces the errors obtained in the first-order isoline, and the accuracy of the asymmetric case is even better than that obtained from the reflectance spectrum using the second-order term. With both simplicity and accuracy, the derived expression can contribute to a wide range of applications, from designing optimal spectral VI sets to developing inversion algorithms in which the derived expression may be used as a constraint in the optimization algorithm.

This study focused on only the relationship between the red and NIR reflectances. Although overcorrections in the NIR band nicely compensated for the truncation errors inherent in the isoline equation, this compensation mechanism may not apply to other combinations of wavelengths. The applicability of this model to other combinations, e.g., the NIR and shortwave bands, will require more thorough investigations. The findings of this study are currently limited to the combination of red and NIR wavelengths.

Overcorrection by intentionally truncating more terms in the red band than in the NIR band compensated for the truncation errors of the higher-order term in a derivation of the vegetation isoline. These findings suggest that optimal control over the overcorrection level could further reduce the errors in the asymmetric isoline. This possibility is worth exploring in future studies.

Acknowledgments

This work was supported by JSPS KAKENHI Grant No. 15H02865.

References

1. J. Qin et al., "Development of the adjoint model of a canopy radiative transfer model for sensitivity study and inversion of leaf area index," *IEEE Trans. Geosci. Remote Sens.* **46**(7), 2028–2037 (2008).
2. A. R. Huete, "A soil-adjusted vegetation index (SAVI)," *Remote Sens. Environ.* **25**(3), 295–309 (1988).
3. F. Baret, G. Guyot, and D. Major, "TSAVI: a vegetation index which minimizes soil brightness effects on LAI and APAR estimation," in *12th Canadian Symposium on Remote Sensing, Int. Geoscience and Remote Sensing Symposium*, Vol. 3, pp. 1355–1358, IEEE (1989).
4. D. Major, F. Baret, and G. Guyot, "A ratio vegetation index adjusted for soil brightness," *Int. J. Remote Sens.* **11**(5), 727–740 (1990).
5. J. Qi et al., "A modified soil adjusted vegetation index," *Remote Sens. Environ.* **48**(2), 119–126 (1994).

6. M. Gilabert et al., "A generalized soil-adjusted vegetation index," *Remote Sens. Environ.* **82**(2), 303–310 (2002).
7. Z. Jiang et al., "Development of a two-band enhanced vegetation index without a blue band," *Remote Sens. Environ.* **112**(10), 3833–3845 (2008).
8. R. Myneni et al., "Global products of vegetation leaf area and fraction absorbed PAR from year one of MODIS data," *Remote Sens. Environ.* **83**(1), 214–231 (2002).
9. R. Darvishzadeh et al., "Inversion of a radiative transfer model for estimating vegetation LAI and chlorophyll in a heterogeneous grassland," *Remote Sens. Environ.* **112**(5), 2592–2604 (2008).
10. J. A. Smith, "LAI inversion using a back-propagation neural network trained with a multiple scattering model," *IEEE Trans. Geosci. Remote Sens.* **31**(5), 1102–1106 (1993).
11. C. Bacour et al., "Neural network estimation of LAI, fAPAR, fCover and LAI × C ab, from top of canopy MERIS reflectance data: principles and validation," *Remote Sens. Environ.* **105**(4), 313–325 (2006).
12. F. Baret et al., "LAI, fAPAR and fCover CYCLOPES global products derived from VEGETATION: Part 1: principles of the algorithm," *Remote Sens. Environ.* **110**(3), 275–286 (2007).
13. S. Jacquemoud et al., "Extraction of vegetation biophysical parameters by inversion of the PROSPECT+ SAIL models on sugar beet canopy reflectance data. Application to TM and AVIRIS sensors," *Remote Sens. Env.* **52**(3), 163–172 (1995).
14. R. B. Myneni et al., "Estimation of global leaf area index and absorbed PAR using radiative transfer models," *IEEE Trans. Geosci. Remote Sens.* **35**(6), 1380–1393 (1997).
15. Y. Knyazikhin et al., "Synergistic algorithm for estimating vegetation canopy leaf area index and fraction of absorbed photosynthetically active radiation from MODIS and MISR data," *J. Geophys. Res.* **103**(D24), 32257–32275 (1998).
16. R. D. Jackson and A. R. Huete, "Interpreting vegetation indices," *Prev. Vet. Med.* **11**(3), 185–200 (1991).
17. F. Baret and G. Guyot, "Potentials and limits of vegetation indices for LAI and APAR assessment," *Remote Sens. Environ.* **35**(2), 161–173 (1991).
18. M. M. Verstraete and B. Pinty, "Designing optimal spectral indexes for remote sensing applications," *IEEE Trans. Geosci. Remote Sens.* **34**(5), 1254–1265 (1996).
19. M. M. Verstraete, B. Pinty, and R. B. Myneni, "Potential and limitations of information extraction on the terrestrial biosphere from satellite remote sensing," *Remote Sens. Environ.* **58**(2), 201–214 (1996).
20. J. Hanes, *Biophysical Applications of Satellite Remote Sensing*, Springer Science & Business Media, Berlin Heidelberg (2013).
21. R. Myneni and D. Williams, "On the relationship between FAPAR and NDVI," *Remote Sens. Environ.* **49**(3), 200–211 (1994).
22. G. Asrar et al., "Theory and applications of optical remote sensing," *Theory Appl. Opt. Remote Sens.* (1989).
23. N. Gobron, B. Pinty, and M. M. Verstraete, "Theoretical limits to the estimation of the leaf area index on the basis of visible and near-infrared remote sensing data," *IEEE Trans. Geosci. Remote Sens.* **35**(6), 1438–1445 (1997).
24. H. Yoshioka et al., "Analysis of vegetation isolines in red-NIR reflectance space," *Remote Sens. Environ.* **74**(2), 313–326 (2000).
25. N. H. Broge and E. Leblanc, "Comparing prediction power and stability of broadband and hyperspectral vegetation indices for estimation of green leaf area index and canopy chlorophyll density," *Remote Sens. Environ.* **76**(2), 156–172 (2001).
26. Z. Jiang et al., "Analysis of NDVI and scaled difference vegetation index retrievals of vegetation fraction," *Remote Sens. Environ.* **101**(3), 366–378 (2006).
27. Z. Jiang et al., "Interpretation of the modified soil-adjusted vegetation index isolines in red-NIR reflectance space," *J. Appl. Remote Sens.* **1**(1), 013503 (2007).
28. H. Yoshioka et al., "Derivation of soil line influence on two-band vegetation indices and vegetation isolines," *Remote Sens.* **1**(4), 842–857 (2009).

29. H. Yoshioka, H. Yamamoto, and T. Miura, "Use of an isoline-based inversion technique to retrieve a leaf area index for inter-sensor calibration of spectral vegetation index," in *IEEE Int. Geoscience and Remote Sensing Symposium*, Vol. 3, pp. 1639–1641, IEEE (2002).
30. A. Kallel et al., "Determination of vegetation cover fraction by inversion of a four-parameter model based on isoline parametrization," *Remote Sens. Environ.* **111**(4), 553–566 (2007).
31. H. Yoshioka, T. Miura, and A. R. Huete, "An isoline-based translation technique of spectral vegetation index using EO-1 Hyperion data," *IEEE Trans. Geosci. Remote Sens.* **41**(6), 1363–1372 (2003).
32. H. Yoshioka, T. Miura, and K. Obata, "Derivation of relationships between spectral vegetation indices from multiple sensors based on vegetation isolines," *Remote Sensing* **4**(3), 583–597 (2012).
33. K. Obata et al., "Derivation of a MODIS-compatible enhanced vegetation index from visible infrared imaging radiometer suite spectral reflectances using vegetation isoline equations," *J. Appl. Remote Sens.* **7**(1), 073467 (2013).
34. H. Yoshioka, A. R. Huete, and T. Miura, "Derivation of vegetation isoline equations in red-NIR reflectance space," *IEEE Trans. Geosci. Remote Sens.* **38**(2), 838–848 (2000).
35. H. Yoshioka, "Vegetation isoline equations for an atmosphere-canopy-soil system," *IEEE Trans. Geosci. Remote Sens.* **42**(1), 166–175 (2004).
36. M. Miura and H. Yoshioka, "Vegetation isoline equations with higher order interaction terms to improve accuracy in retrieval of vegetation biophysical parameters," in *IEEE Int. Geoscience and Remote Sensing Symposium*, Vol. 3, p. 1056, IEEE (2008).
37. M. Miura, K. Obata, and H. Yoshioka, "Vegetation isoline equations for analysis of hyperspectral data with higher order interaction terms," in *IEEE Int. Geoscience and Remote Sensing Symposium*, pp. 1031–1034, IEEE (2010).
38. M. Miura, K. Obata, and H. Yoshioka, "Vegetation isoline equations for atmosphere-canopy-soil system of layer with second order interaction term," *Proc. SPIE* **7809**, 780906 (2010).
39. S. Jacquemoud et al., "PROSPECT+ SAIL models: a review of use for vegetation characterization," *Remote Sens. Environ.* **113**, S56–S66 (2009).
40. K. Cooper, J. Smith, and D. Pitts, "Reflectance of a vegetation canopy using the adding method," *Appl. Opt.* **21**(22), 4112–4118 (1982).
41. F. Baret, S. Jacquemoud, and J. Hanocq, "The soil line concept in remote sensing," *Remote Sens. Rev.* **7**(1), 65–82 (1993).
42. S. Jacquemoud and F. Baret, "PROSPECT: a model of leaf optical properties spectra," *Remote Sens. Environ.* **34**(2), 75–91 (1990).
43. W. Verhoef, "Earth observation modeling based on layer scattering matrices," *Remote Sens. Environ.* **17**(2), 165–178 (1985).

Munenori Miura is a PhD student at Aichi Prefectural University, Aichi, Japan. He received his BS and MS degrees in information science and technology from Aichi Prefectural University in 2008 and 2010, respectively.

Kenta Obata is a researcher in the Institute of Geology and Geoinformation at the National Institute of Advanced Industrial Science and Technology, Japan. He received his MS and PhD degrees in information science and technology from Aichi Prefectural University, Aichi, Japan, in 2010 and 2012, respectively. His research interests include intersensor calibration of biophysical retrievals, spectral mixture analysis, and radiometric calibration.

Hiroki Yoshioka is a professor in the Department of Information Science and Technology at Aichi Prefectural University, Aichi, Japan. He received his MS and PhD degrees in nuclear engineering from the University of Arizona, Tucson, in 1993 and 1999, respectively. His research interests include cross-calibrations of satellite data products for continuity and compatibility of similar data sets, and development of canopy radiative transfer models and their inversion techniques.